PAPER

Check for updates

Upconversion fluorescence of MXene nanosheets and the sensitive detection of L-tryptophan†

Feng Wang,[ac] Hongye Wang,[a] Xiaoqiang Cui [iD] *[b] and Yang Liu [iD] *[a]

Innovating the fluorescence characteristic of MXene nanosheets and quantum dots could result in fascinating perspectives in the applications of sensing, imaging and photocatalysis. However, the currently reported MXene-based materials have only shown down-conversion fluorescence emission, while the exploration and research of up-conversion fluorescent performance are scarce. Herein, the upconversion emission behaviors of Ti_3C_2 MXene nanosheets are reported and investigated for the first time. It was observed that the Ti_3C_2 nanosheets present upconversion emission in a wide wavelength range with adjustable color, covering almost the entire visible spectrum. The unique features of larger anti-stokes displacement (over 200 nm), narrower full width at half maximum (~17 nm) and longer lifetime (1.18 μs) were also exhibited, which are superior to those of the down-conversion fluorescence. The self-quenched fluorescence of the Ti_3C_2 nanosheets on the side of the highest fluorescence emission was also displayed. Based on the quenching effect of L-tryptophan on the Ti_3C_2 fluorescence by a fast charge transfer mechanism, a fast, simple and label-free fluorescence sensor for L-tryptophan detection was realized with a detection limit as low as 91 nM, which provides a valuable tool to widen their applications in food safety and diagnostics.

Introduction

Transition metal carbides/nitrides (MXenes), as novel inorganic 2D materials, have recently become a hot research area.[1–4] Researchers have demonstrated that MXenes possess super performances, such as high metallic conductivity of 2400 S cm^{-1} and excellent hydrophilicity induced by terminated hydrophilic groups of –OH or –F on the surface.[5–7] These special features, which distinguished them from those of traditional 2D materials, synergistically endow MXenes with intercalation or surface redox capacitances, greatly promoting their application potential in batteries,[8] supercapacitors,[9] and pollutant disposal.[10] Furthermore, reducing their size to nanosheets or nanodots can endow them with extremely useful optical properties and functions because of the quantum confinement effect, which makes MXenes promising candidates for imaging,[11,12] sensors,[13,14]

[a] Department of Chemistry, Key Laboratory of Bioorganic Phosphorus Chemistry & Chemical Biology, Tsinghua University, Beijing 100084, P. R. China. E-mail: liu-yang@mail.tsinghua.edu.cn

[b] School of Materials Science and Engineering, State Key Laboratory of Automotive Simulation and Control and Key Laboratory of Automobile Materials of MOE, Jilin University, 2699 Qianjin Street, Changchun 130012, Jilin, China

[c] Shenzhen Key Laboratory of Energy Materials for Carbon Neutrality, Shenzhen Institutes of Advanced Technology, Chinese Academy of Sciences, Shenzhen, 518055, China

† Electronic supplementary information (ESI) available. See DOI: https://doi.org/10.1039/d2sd00107a

and photoelectric conversion.[15] For instance, based on down-conversion fluorescence, it can be used as an intracellular pH sensor[16] or for the highly sensitive analysis of hypochlorite,[17] as well as the label-free detection and imaging of metal ions.[18] The heterostructure composed of MXene quantum dots and Cu_2O nanowires was developed for boosting the photocatalytic reduction of CO_2 into methanol.[19] Although the study of the optical application from MXenes has made significant progress, some drawbacks have been accompanied by the fact that the excitation and emission wavelengths of down-conversion fluorescence are always shorter, usually less than 500 nm. For photocatalysis, the energy in the visible and infrared regions may be squandered, resulting in low catalytic activity. For bio-analysis, it is hard to avoid fluorescence interference caused by cellular autofluorescence at nearby wavelengths, which is also harmful to animal and human cells to some extent.

Upconversion luminescent materials are of great interest to analytical chemists, optical device engineers, and biologists and have achieved considerable development.[20–23] Common upconversion luminescent materials consist of two-dimensional materials such as graphene,[24] some quantum dots[25] and rare earth materials.[26–28] They have been used as fluorescent probes for the detection and imaging of tumors[29] and quantification of microRNA in living cells.[30] These studies suggest that upconversion materials tend to have longer excitation wavelength and emission wavelength,

enabling more sensitive biological analysis and imaging with a higher signal-to-noise ratio, which could avoid fluorescence interference from cellular autofluorescence and enable less damage to cells. However, the relevant information from MXenes-based upconversion fluorescence is rarely reported. Combined with the above excellent features of MXenes with high biocompatibility, exploiting and revealing their upconversion fluorescence behaviors for reducing background fluorescence interference and developing a new signal conversion mechanism will, to some extent, provide promising potential in boosting biosensors and imaging.

In this study, we successfully synthesized MXene (Ti_3C_2) nanosheets with a few layers. The upconversion luminescence of the Ti_3C_2 nanosheets was observed for the first time, which presented unique features of wide spectral coverage from 450 nm to 600 nm with a narrow full width at half maximum (FWHM) of 17 nm, and a long fluorescence lifetime of about 1.18 μs. An emission mechanism of the upconversion luminescence of the Ti_3C_2 nanosheet was demonstrated. Given the excellent properties of the Ti_3C_2 nanosheets, a fluorescence sensor was developed for the analysis of L-tryptophan, which is an essential amino acid for the human body and its deficiency can cause skin disorders, cataracts, vitreous degeneration and myocardial fibrosis.[31,32] Selective fluorescence quenching of the Ti_3C_2 nanosheets was observed in the presence of L-tryptophan. The fluorescence sensor showed high sensitivity and excellent selectivity with a limit of detection (LOD) as low as 91 nM. The excellent features of the upconversion luminescence of MXene showed great prospects in food analysis, disease diagnostics and therapies.

Materials and methods

Materials

Lithium fluoride (LiF), 50% hydrofluoric acid solution (HF), tetramethylammonium hydroxide (TMAOH), glutathione, L-histidine, alanine, L-cysteine, L-tryptophan, vitamin H, L-serine, urea, citric acid, L-lactic acid, and hydroxylamine were purchased from Aladdin Industrial Inc. Maltose, L-arginine, biphenyl, melamine, L-tyrosine, glycine and L-lysine were acquired form Macklin Inc. The Ti_3AlC_2 powders were purchased from Jilin Technology Co. Ltd. The 12 mol L^{-1} hydrochloric acid solution was obtained from Beijing Chemical Plant. All chemicals (A.R. grade) were used without further treatment.

Preparation of Ti_3C_2 nanosheets by HCl/LiF

In the preparation of Ti_3C_2 nanosheets, as previously reported,[6] 15 mL of hydrochloric acid and 2 g of LiF were mixed in a Teflon reactor and stirred for 15 minutes until completely dissolved. Then, 2 g Ti_3AlC_2 powder was slowly added to the mixture for about 20 min. The mixed liquid was stirred at a constant temperature of 40 °C for 24 hours in a closed reactor. The reaction solution was added to distilled water, and washed several times with centrifugation. The

rotation speed was increased from 3500 rpm until the supernatant achieved pH >6, and then the whole supernatant was decanted. After adding distilled water and ultrasound for one hour, the mixture was centrifuged for one hour at 3500 rpm, and the supernatant was collected and freeze-dried to obtain powdery Ti_3C_2 nanosheets.

Preparation of S–Ti_3C_2

The S–Ti_3C_2 nanosheets were prepared based on previous reports.[33,34] Here, 1 g of Ti_3AlC_2 was added slowly to 15 mL of 50% hydrofluoric acid solution within 20 minutes. The mixture solution was transferred to a Teflon reactor and stirred at a constant temperature of 35 °C for 24 hours. After the solution was cleaned by centrifugation several times until pH >6, the precipitate was placed in a vacuum drying oven and dried for 18 hours to obtain accordion-like Ti_3C_2. Afterwards, the obtained accordion-like Ti_3C_2 was added to the TMAOH solution. After stirring for 24 hours at room temperature, the mixed solution was centrifuged several times, and the supernatant was decanted until the final pH was <8. The resulting solution was shaken well and, finally, S–Ti_3C_2 was obtained after freeze-drying. It is worth noting that during each centrifugation process, after adding the distilled water solution for precipitation, just gently shaking the solution was required.

Apparatus and characterizations

The morphology was determined using a scanning electron microscope (SEM) (Hitachi SU8010) operated at 5 kV, and a transmission electron microscope (TEM) (JEM-2000F) from JEOL Co., Japan. The thickness of the nanosheets was measured via atomic force microscopy (AFM) (Dimension Icon, Bruker, Germany) under the tapping mode in air. X-ray diffraction (XRD) was conducted at a scanning rate of 5° min^{-1} using a Bruker D8 diffractometer with 1.5418 Å Cu Kα radiation. The Raman spectra were acquired by a Smart Raman Spectrometer (LABRAM ARAMIS) with the laser sources under 633 nm excitation at ambient temperature. The FT-IR spectra were obtained by CDS-2000 Bio-Rad FTS-165 FT-IR apparatus. The elemental analysis of the samples was conducted via X-ray photoelectron spectroscopy (XPS) using an Escalab-250 instrument (Thermo Fisher Scientific, USA) with a hemisphere detector and a monochromatic Al Kα radiation source (1486.6 eV). The photoluminescence (PL) spectra were obtained using an LS55 spectrometer (PerkinElmer Inc., USA). Photoluminescence decay was measured using an Edinburgh FLS920 instrument. The test principle was Time-Correlated Single Photon Counting (TCSPC). The repetition frequency was 40 kHz, and the spectral resolution was 0.05 nm.

Calculation of fluorescence lifetimes

The fluorescence decay curves in this article were fitted by a double-exponential function:[35]

$$y = A_1 e^{-(t/\tau_1)} + A_2 e^{t/\tau_2}$$

The average lifetimes were calculated using the average lifetime model:

$$\tau = \frac{\in A_n \tau_n^2}{A_n \tau_n} \quad (n = 1, 2, 3......)$$

Construction of an L-tryptophan sensing platform based on Ti_3C_2 nanosheets

The Ti_3C_2 nanosheets-based Ti_3C_2 nanosheets detection platform was established as follows: 80 μL of Ti_3C_2 nanosheet solution was added to 100 μL phosphatic buffer solution (0.1 M, pH = 7.4), then 20 μL of L-tryptophan solution with various concentrations was mixed and incubated for 6 min at room temperature. The fluorescence performances of Ti_3C_2 aqueous solution mixed with 3 μM various small organic molecules, including other amino acids (alanine, L-histidine, glutathione, L-cysteine, L-lysine, hydroxylamine, melamine, glycine, L-tyrosine, L-arginine, L-serine, biphenyl, maltose,

urea, citric acid, L-lactic acid, vitamin H) were investigated as the selectivity experiments.

Detection of L-tryptophan in real samples based on L-tryptophan

To confirm the reliability of the sensor, L-tryptophan analysis in human serum was performed. Human serum was purchased from Kejing Biological Technology Co. Ltd. (Jiangsu, China). The content of L-tryptophan was determined by the standard addition method. Briefly, human serum solution was produced by diluting the serum sample 100 times with 1 X PBS (pH 7.4). Here, 10.0 μL Ti_3C_2 nanosheets (4 mg mL^{-1}) and different amounts of L-tryptophan were mixed and diluted with the serum solution for a total volume of 10 mL.

Results and discussion

The characterization of Ti_3C_2 nanosheets

The Ti_3C_2 nanosheets were obtained by etching Ti_3AlC_2 with a mixed solution of LiF and HCl, repeated shaking and sonicating the resulting solution. The structures and
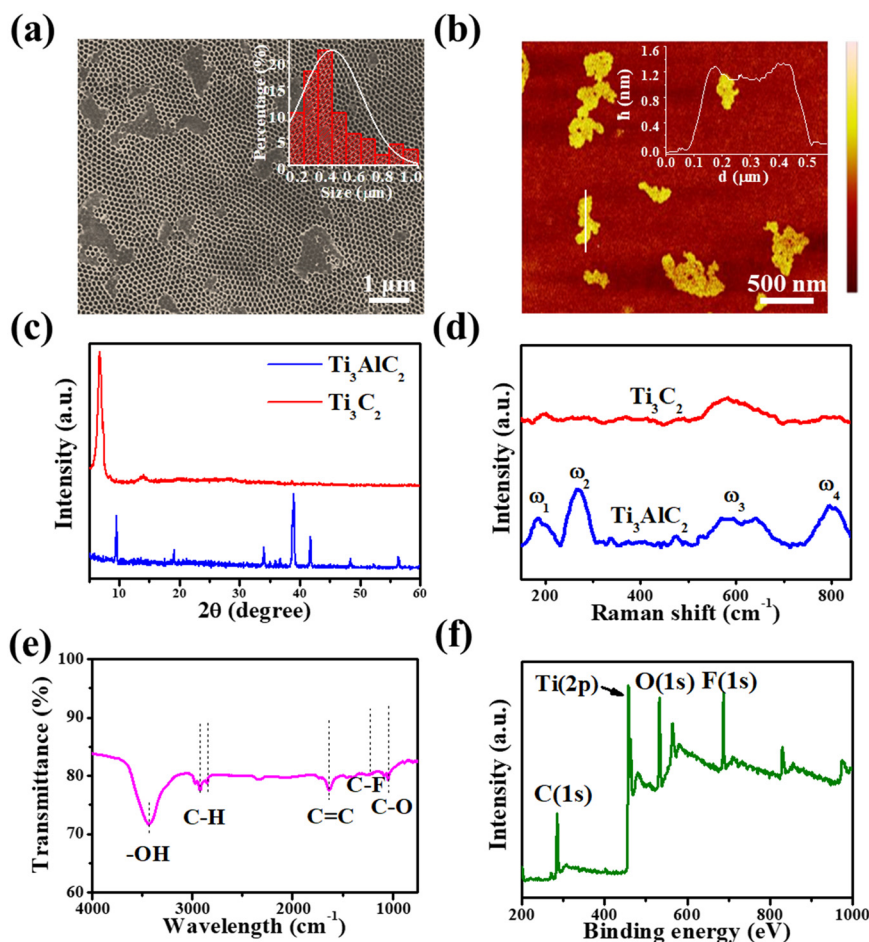

Fig. 1 (a) SEM image of Ti_3C_2 nanosheets on AAO (inset shows the fitted normal distribution curve). (b) AFM topography image of Ti_3C_2 nanosheets. (c) XRD patterns of Ti_3AlC_2 and Ti_3C_2 nanosheets. (d) Raman spectrum of Ti_3AlC_2 and Ti_3C_2 nanosheets. (e) FTIR spectrum of Ti_3C_2 nanosheets. (f) XPS spectrum of Ti_3C_2 nanosheets.

morphologies of the as-prepared nanosheets were identified by SEM and AFM images, as shown in Fig. 1a and b. It was observed that ultra-thin nanosheets were obtained (Fig. 1a). As shown in the inset of Fig. 1a, the size of the nanosheets was *ca.* 400 nm. The Ti_3C_2 nanosheets can also be observed from the TEM images (Fig. S1†).

The AFM image shows that the average thickness of Ti_3C_2 nanosheets is nearly 1 nm (Fig. 1b), which means that they are monolayer nanosheets. The XRD patterns of powdered Ti_3AlC_2 and as-exfoliated Ti_3C_2 nanosheets are shown in Fig. 1c. The sharp XRD peak at 39°, compared to that of Ti_3AlC_2, disappeared in the pattern of Ti_3C_2 nanosheets, indicating that the interlayer Al of Ti_3AlC_2 was successfully etched by LiF/HCl solution. The peak position of the XRD diffraction peaks shifted to a small diffraction angle at about 7°, which may be ascribed to the formation of the single-layer structure of Ti_3C_2.[36] Fig. 1d shows the Raman spectra of Ti_3AlC_2 and Ti_3C_2 nanosheets; the first two peaks in the

spectrum of Ti_3AlC_2, ω_1 and ω_2, could be attributed to the vibrations of Ti–Al, and the other two peaks (ω_3 and ω_4) at 579 cm^{-1} and 800 cm^{-1} originated from the vibrations of Ti–C. For the spectrum of Ti_3C_2 nanosheets, ω_1 and ω_2 disappeared and ω_3 and ω_4 remained, which also means that Al was removed. The FTIR spectrum of the as-exfoliated Ti_3C_2 nanosheets is shown in Fig. 1e, which exhibits a broad band around 3430 cm^{-1} corresponding to the –OH stretching vibration. Other FTIR bands at 1050 cm^{-1}, 1110 cm^{-1}, 1640 cm^{-1}, 2850 cm^{-1} and 2925 cm^{-1} corresponded to the stretching vibrations of CO, C–F, C=C and C–H, respectively. These results indicate that a large number of functional groups, such as –OH and –F exist on the surface and sides of the Ti_3C_2 nanosheets. The nature of the chemical bonds can be determined by XPS, which is shown in Fig. 1f. The peaks in the XPS survey spectrum correspond to C 1s, O 1s, F 1s and Ti 2p, respectively. For the high-resolution spectrum of C 1s (Fig. S2†), the five deconvoluted peaks corresponded to
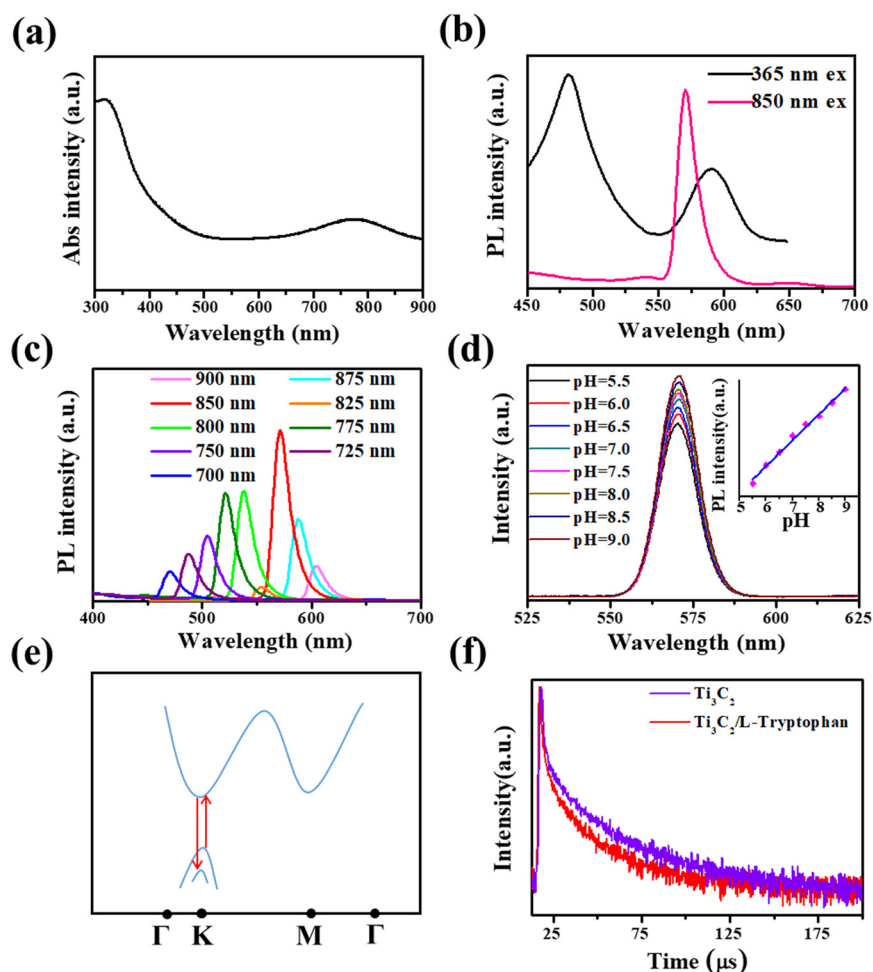
Fig. 2 (a) UV-vis absorption of Ti_3C_2 nanosheets. (b) Fluorescence emission spectra of Ti_3C_2 nanosheets. (c) Fluorescence emission spectra of Ti_3C_2 nanosheets with different excitation wavelengths from 700 nm to 900 nm. (d) Fluorescence emission of Ti_3C_2 nanosheets with different pH values ranging from 5.5 to 9.0. The inset is the relationship of the PL intensity *vs.* the value of pH. (e) Schematic band structure of the electron transition process of Ti_3C_2 nanosheets. (f) Photoluminescence decay of an aqueous solution of Ti_3C_2 nanosheets before and after adding L-tryptophan.

C=O, C–O, C–C, C–Ti–O, C–Ti, respectively.[37] These results further support the existence of –O, –F and –OH terminations on the surface of the as-prepared Ti_3C_2 nanosheets.

The optical properties of Ti_3C_2 nanosheets

Fig. 2a shows the UV-vis absorption spectrum of the as-exfoliated Ti_3C_2 nanosheets, and there is a typical absorption peak at 330 nm. According to the results of first-principles density functional theory (DFT) calculations previously reported,[38] the absorption peak at 330 nm can be attributed to the trapping of the surface excited state energy of Ti_3C_2 nanosheets. A peak was also observed at about 800 nm, attributed to the surface plasmon resonance of Ti_3C_2 nanosheets.[39] The fluorescence emission spectra of Ti_3C_2 nanosheets in an aqueous solution with excitation wavelengths of 365 nm and 850 nm are shown in Fig. 2b. A fluorescence peak at 480 nm was observed at the excitation wavelength of 365 nm, due to the Stokes PL mechanism.[40] It is interesting that an up-conversion fluorescence emission peak at 570 nm at the excitation wavelength of 850 nm was observed, which presented a narrower FWHM of 17 nm and was superior to most reported inorganic luminescent materials.[35,41] In addition, both down-conversion and upconversion emission demonstrated excitation wavelength-dependent behaviors, as shown in Fig. S3† and 2c. The emission peak can be obtained from 465 nm to 605 nm by changing the excitation wavelength from 700 nm to 900 nm (Fig. 2c). Unexpectedly, at the excitation wavelength of 825 nm, the luminescence intensity had a sharp decline in the emission spectra. The excitation wavelength of 825 nm is close to that with the strongest intensity and is located in the plasmonic absorption range. Therefore, we speculate that the abnormal quenching effect, named the "interruption effect" herein, may result from the inner filter effect induced by the absorption of the surface plasmonic peak.[42] Although the excitation wavelength-dependent behavior for down-conversion is similar to that of Ti_3C_2 quantum dots, this is the first report on the up-conversion emission behavior of Ti_3C_2 nanosheets. More importantly, the observed interruption effect will offer a great opportunity to enhance image resolution and sensor sensitivity because adjacent fluorescence quenching greatly reduces the interference to the optical application based on the highest emission peak.

Neither Ti_3AlC_2 powder nor the accordion-like Ti_3C_2 has a fluorescence peak at 850 nm excitation (Fig. S4†), which possibly means that the upconversion luminescence only occurs when the dimensions are reduced to two dimensions or lower. Moreover, the larger size and multiple functional groups of the light-emitting Ti_3C_2, compared to other two-dimensional materials previously reported,[35,41,43] may suggest the potential of multifunctional attachments in the development of novel probes. The energies of emission light and excitation light have a good linear relationship, whose fit line can be expressed as $y = 1.48x + 0.01$ eV ($R^2 = 0.99995$) (Fig. S5†). This indicates that the conventional anti-Stokes PL

mechanism induces up-conversion luminescence.[35] To further study its luminescence properties, we investigated the effect of pH on PL emission behaviors in the Ti_3C_2 nanosheets at the excitation wavelength of 850 nm. The PL intensity of Ti_3C_2 nanosheets gradually increased with the pH changing from 5.5 to 9.0, as shown in the fluorescence emission spectra from Fig. 2d. The inset in Fig. 2d shows a good linear relationship between the peak intensity and the pH in aqueous solutions, and the PL intensity increased gradually with the increase in pH value. This can be attributed to the large amount of –OH groups that existed on the surface of the Ti_3C_2 nanosheets. The –OH group not only suppresses non-radiative processes, they also perfect the integrity of the π-conjugated system as an electron donor, resulting in the enhancement of the PL intensity.[39] The previous reports have pointed out that Ti_3C_2 nanosheets have a direct band gap, similar to that of MoS_2 quantum dots[44,45] and graphene quantum dots.[46,47] Therefore, a similar energy band structure and anti-Stokes PL mechanism were presented, as shown in Fig. 2e. Through absorbing photon energy from irradiation, the electrons transfer from the highest occupied molecular orbital (HOMO) to the lowest unoccupied molecular orbital (LUMO), forming excited electrons. Then, the excited electrons get down to a lower energy state than the HOMO, releasing higher energy than the absorbed photon energy, which leads to an upconversion behavior. The photoluminescence decay curve of an aqueous solution of Ti_3C_2 nanosheets in the process of upconversion luminescence is shown in Fig. 2f. The spectrum fit very well as a double exponential decay curve (the pink curve in the figure), and the average lifetime of the as-prepared Ti_3C_2 was calculated to be 1.18 μs.

The upconversion luminescence of Ti_3C_2 nanosheets with different synthetic paths

To investigate whether synthetic paths affect the presence of upconversion luminescence behaviors, we also chose another way to get Ti_3C_2 nanosheets. Ti_3AlC_2 were etched with HF, and then exfoliated with TMAOH (S–Ti_3C_2 NPs). S–Ti_3C_2 NPs also exhibited down-conversion fluorescence emission and upconversion fluorescence emission, just like the Ti_3C_2 nanosheets prepared by LiF and HCl. The fluorescence spectra of S–Ti_3C_2 NPs could be modulated by changing the excitation light wavelength (Fig. S6†). It could be summarized that the Ti_3C_2 nanosheets with upconversion luminescence properties could be prepared in different ways, and the upconversion phenomena are similar. The upconversion-emitted light intensity of S–Ti_3C_2 NPs was significantly higher than that of Ti_3C_2 nanosheets at 850 nm excitation (Fig. S7†), which can also be attributed to more –OH groups on the surface of nanosheets, similar to the previous report. Therefore, we can propose that Ti_3C_2 nanosheets with –OH groups may all exhibit their own upconversion behaviors with excitation dependence. In addition, the up-conversion emission behaviors from other MXene nanosheets or
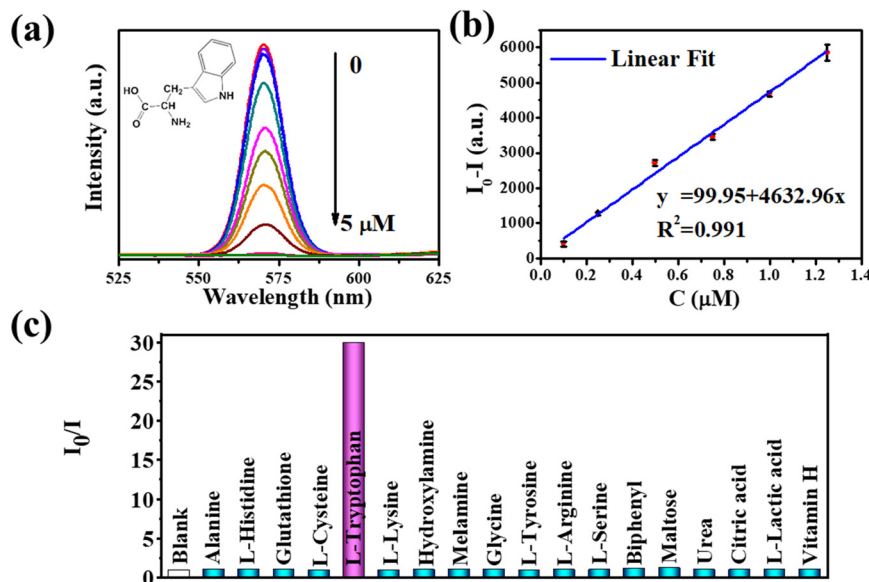
Fig. 3 (a) Fluorescence intensity response of the Ti$_3$C$_2$ solution with different concentrations of L-tryptophan from 0 to 500 nM at 850 nm excitation. (b) The relationship of the intensity of the initial fluorescence (I_0) *vs.* that of the actual fluorescence (I) with the concentration of L-tryptophan. (c) The response histogram of the fluorescence intensity of Ti$_3$C$_2$ depending on various reagents at 3 μM.

quantum dots will become worthy of study as new subjects in order to develop fluorescence probes with higher efficiency in the future.

The detection of L-tryptophan based on up-conversion fluorescence

L-Tryptophan is an essential amino acid for the human body and its deficiency can cause phenylketonuria, cataracts, depression, and myocardial fibrosis.[31,32,48] Furthermore, the photoluminescence decay of Ti$_3$C$_2$ nanosheets after mixing with L-tryptophan was also tested, as shown in the red curve of Fig. 2f. A shorter average lifetime of about 267 ns was observed, compared with that of Ti$_3$C$_2$ nanosheets, which means that a faster charge transfer process takes place from Ti$_3$C$_2$ nanosheets to L-tryptophan, causing the fluorescence quenching of the Ti$_3$C$_2$ nanosheets.[49] In this study, based on the quenching effect of L-tryptophan on up-conversion emission, we developed the Ti$_3$C$_2$ nanosheets as a novel fluorescent probe with no label to directly detect L-tryptophan. Based on the optimal experimental conditions (Fig. S8 and S9†), 4 μg mL^{-1} Ti$_3$C$_2$ nanosheets and 6 min incubation time were selected for constructing the L-tryptophan sensor. As shown in Fig. 3a, the upconversion fluorescence intensity of the Ti$_3$C$_2$ decreased significantly, with gradually increasing the concentration of the L-tryptophan from 0 to 5 μM, until it was almost completely quenched. Fig. 3b shows the variation in the difference between the initial fluorescence intensity and the actual fluorescence intensity at 570 nm ($I_0 - I$) in the presence of different concentrations of L-tryptophan. The spectra show that $I_0 - I$ has a good linear relationship with the concentrations of L-tryptophan in the range from 0–5 μM.

The fit line can be expressed as $y = 99.95 + 4632.96x$ (where $R^2 = 0.991$, y is $I_0 - I$, x is the concentration of L-tryptophan), and the detection limit of L-tryptophan was calculated to be as low as 91 nM, which is comparable with those reported in the literature (Table S1†).

We also investigated the fluorescence performance of various small organic molecules at a concentration of 3 μM, including other amino acids mixed with Ti$_3$C$_2$ aqueous solution, as shown in Fig. 3c. At this concentration, the addition of L-tryptophan to the Ti$_3$C$_2$ aqueous solution significantly quenched the fluorescence. While it does not exhibit such properties for other types of organic molecules at the same concentration, their fluorescence emission intensity is basically the same as I_0, which suggests that Ti$_3$C$_2$ aqueous solution has good specificity for L-tryptophan. In addition, to evaluate the applicability of L-tryptophan detection based on Ti$_3$C$_2$ nanosheets, the sensor was also applied in the detection of L-tryptophan in human serum samples. As displayed in Table 1, the results validated that the recoveries of the added L-tryptophan were maintained between 95.6% and 103%, demonstrating the potential application of Ti$_3$C$_2$ in real sample detection. These results suggest that these nanosheets are very suitable for use as fluorescent molecular probes for detecting L-tryptophan.

Table 1 Determination of L-tryptophan in human serum samples

L-Trp added (μM)	L-Trp found (μM)	Recovery (%)	RSD (%, $n = 3$)
0.1	0.103	103	2.1
0.5	0.478	95.6	3.7
2.0	1.944	97.2	2.9

Conclusion

In conclusion, we have successfully synthesized Ti_3C_2 nanosheets with a few layers and confirmed their upconversion luminescence properties. The upconversion luminescence phenomenon of Ti_3C_2 nanosheets has wide spectral coverage, a narrow FWHM, and a long fluorescence lifetime. The self-quenching of upconversion fluorescence was found and reported. Based on the upconversion property, we have developed Ti_3C_2 nanosheets as fluorescent molecular probes for the detection of L-tryptophan. The detection limit of this fluorescent molecular probe was as low as 91 nM and of excellent selectivity. This report adds to the upconversion luminescent materials, and the advantages of upconversion of Ti_3C_2 nanosheets also provide MXenes with great potential for more biological applications.

Author contributions

Feng Wang: investigation, methodology, conceptualization, writing-original draft, writing-review & editing; Hongye Wang: writing-review & editing, analysis, suggestion; Xiaoqiang Cui, Yang Liu: methodology, validation, resources, data curation, supervision, project administration, writing-review & editing, funding acquisition.

Conflicts of interest

The authors declare no competing financial interest.

Acknowledgements

References

1 S. K. Bhardwaj, H. Singh, M. Khatri, K. H. Kim and N. Bhardwaj, *Biosens. Bioelectron.*, 2022, **202**, 113995.

2 Y. J. Wu, Y. J. Sun, J. F. Zheng, J. H. Rong, H. Y. Li and L. Niu, *Chem. Eng. J.*, 2021, **404**, 126565.

3 D. P. Huang, H. H. Yu and H. J. Zhang, *Gaodeng Xuexiao Huaxue Xuebao*, 2021, **42**, 397–411.

4 M. M. Hu, H. Zhang, T. Hu, B. B. Fan, X. H. Wang and Z. J. Li, *Chem. Soc. Rev.*, 2020, **49**, 6666–6693.

5 B. Anasori, M. R. Lukatskaya and Y. Gogotsi, *Nat. Rev. Mater.*, 2017, **2**, 16098.

6 Y. Xia, T. S. Mathis, M. Q. Zhao, B. B. Anasori, A. Dang, Z. H. Zhou, H. Cho, Y. Gogotsi and S. Yang, *Nature*, 2018, **557**, 409.

7 Z. H. Bao, C. G. Lu, X. Cao, P. G. Zhang, L. Yang, H. Zhang, D. W. Sha, W. He, W. Zhang, L. Pan and Z. G. Sun, *Chin. Chem. Lett.*, 2021, **32**, 2648–2658.

8 F. W. Ming, H. F. Liang, G. Huang, Z. Bayhan and H. N. Alshareef, *Adv. Mater.*, 2021, **33**, 2004039.

9 N. Kurra, B. Ahmed, Y. Gogotsi and H. N. Alshareef, *Adv. Energy Mater.*, 2016, **6**, 1601372.

10 S. K. Hwang, S. M. Kang, M. Rethinasabapathy, C. Roh and Y. S. Huh, *Chem. Eng. J.*, 2020, **397**, 1254.

11 Q. Xue, H. J. Zhang, M. S. Zhu, Z. X. Pei, H. F. Li, Z. F. Wang, Y. Huang, Y. Huang, Q. H. Deng, J. Zhou, S. Y. Du, Q. Huang and C. Y. Zhi, *Adv. Mater.*, 2017, **29**, 1604847.

12 X. Yan, J. F. Ma, K. X. Yu, J. P. Li, L. Yang, J. Q. Liu, J. C. Wang and L. L. Cai, *Chin. Chem. Lett.*, 2020, **31**, 3173–3177.

13 D. H. Ho, Y. Y. Choi, S. B. Jo, J. M. Myoung and J. H. Cho, *Adv. Mater.*, 2021, **33**, 2005846.

14 B. Wang, S. P. Zhong, P. Xu and H. Zhang, *Chem. Eng. J.*, 2021, **403**, 126336.

15 S. Z. Li, J. F. Ma, X. L. Zhao, P. D. Zhu, Xu Meng, Y. C. Niu, D. X. Luo and Q. Xu, *Chin. Chem. Lett.*, 2022, **33**, 1850–1854.

16 X. Chen, X. Sun, W. Xu, G. Pan, D. Zhou, J. Zhu, H. Wang, X. Bai, B. Dong and H. Song, *Nanoscale*, 2017, **10**, 1111–1118.

17 M. Liu, Y. Bai, Y. He, J. Zhou, Y. Ge, J. Zhou and G. Song, *Microchim. Acta*, 2021, **188**, 15.

18 Q. Zhang, Y. Sun, M. Liu and Y. Liu, *Nanoscale*, 2020, **12**, 1826–1832.

19 Z. P. Zeng, Y. B. Yan, J. Chen, P. Zan, Q. H. Tian and P. Chen, *Adv. Funct. Mater.*, 2019, **29**, 1806500.

20 Z. Jing, L. Qian, W. Feng, Y. Sun and F. Li, *Chem. Rev.*, 2014, **115**, 395–465.

21 D. L. Liang, Q. H. Song, Y. T. Yao and B. Liu, *Gaodeng Xuexiao Huaxue Xuebao*, 2019, **40**, 583–591.

22 J. W. Zhu, J. J. Shen, B. Hu, L. Yang and C. L. Jiang, *Anal. Chem.*, 2022, **94**, 1126–1134.

23 J. W. Zhu, B. Hu, L. Yang and C. L. Jiang, *Sens. Actuators, B*, 2021, **345**, 130378.

24 D. D. Su, X. Zhao, X. Yan, X. S. Han, Z. F. Zhu, C. G. Wang, X. T. Jia, F. M. Liu, P. Sun, X. M. Liu and G. Y. Lu, *Biosens. Bioelectron.*, 2021, **194**, 113598.

25 Q. Zhang, D. Jie, Y. Shen, D. Chen, Q. Zhou, Q. Chen, Z. He and J. Qiu, *J. Alloys Compd.*, 2010, **508**, 13–15.

26 L. Xiong, Z. Chen, Q. Tian, T. Cao, C. Xu and F. Li, *Anal. Chem.*, 2009, **81**, 8687–8694.

27 X. W. Liu, M. Liu, J. J. Chen, Z. H. Li and Q. Yuan, *Chin. Chem. Lett.*, 2018, **29**, 1321–1332.

28 B. Hu, J. W. Zhu, J. J. Shen, L. Yang and C. L. Jiang, *Anal. Chem.*, 2022, **94**, 7559–7566.

29 S. Y. Choi, S. H. Baek, S. J. Chang, Y. Song, R. Rafique, K. T. Lee and T. J. Park, *Biosens. Bioelectron.*, 2017, **93**, 267–273.

30 S. Li, L. G. Xu, W. Ma, X. L. Wu, M. Z. Sun, H. Kuang, L. B. Wang, N. A. Kotov and C. L. Xu, *J. Am. Chem. Soc.*, 2016, **138**, 306–312.

31 C. Mainetti, M. Fathi and J. H. Saurat, *Dermatology*, 1991, **183**, 62–65.

32 D. M. Richard, M. A. Dawes, C. W. Mathias, A. Acheson, N. Hill-Kapturczak and D. M. Dougherty, *Int. J. Tryptophan Res.*, 2009, **2**, 45–60.

33 M. Alhabeb, K. Maleski, B. Anasori, P. Lelyukh, L. Clark, S. Sin and Y. Gogotsi, *Chem. Mater.*, 2017, **29**, 7633–7644.

34 O. Mashtalir, M. Naguib, V. N. Mochalin, Y. Dall'Agnese, H. Min, M. W. Barsoum and Y. Gogotsi, *Nat. Commun.*, 2013, **4**, 1716.

35 H. Dong, S. Tang, Y. Hao, H. Yu, W. Dai, G. Zhao, Y. Cao, H. Lu, X. Zhang and H. Ju, *ACS Appl. Mater. Interfaces*, 2016, **8**, 3107–3114.

36 Q. Tang, Z. Zhen and P. Shen, *J. Am. Chem. Soc.*, 2012, **134**, 16909–16916.

37 Y. L. Qin, Z. Q. Wang, N. Y. Liu, Y. Sun, D. X. Han, Y. Liu, L. Niu and Z. H. Kang, *Nanoscale*, 2018, **10**, 14000–14004.

38 Q. Xu, L. Ding, Y. Y. Wen, W. J. Yang, H. J. Zhou, X. Z. Chen, J. Street, A. G. Zhou, W. J. Ong and N. Li, *J. Mater. Chem. C*, 2018, **6**, 6360–6369.

39 J. K. Demellawi, S. Lopatin, J. Yin, O. F. Mohammed and H. N. Alshareef, *ACS Nano*, 2018, **12**, 8485–8493.

40 Q. X. Zhang, F. Wang, H. X. Zhang, Y. Y. Zhang, M. L. Liu and Y. Liu, *Anal. Chem.*, 2018, **90**, 12737–12744.

41 S. Zhuo, M. Shao and S. T. Lee, *ACS Nano*, 2012, **6**, 1059–1064.

42 Q. Hua, L. Gao, S. Q. Rao, Z. Q. Yang, T. Li and X. J. Gong, *Food Chem.*, 2019, **280**, 195–202.

43 R. Furue, K. Matsuo, Y. Ashikari and H. Ooka, *Adv. Opt. Mater.*, 2018, **6**, 1701147.

44 T. Guo, L. N. Wang, S. Sun, Y. Wang, X. L. Chen, K. N. Zhang, D. X. Zhang, Z. H. Xue and X. B. Zhou, *Chin. Chem. Lett.*, 2019, **30**, 1253–1260.

45 X. Zhu, J. Xiang, J. Li, C. Feng, P. Liu and B. Xiang, *J. Colloid Interface Sci.*, 2017, **511**, 209–214.

46 S. Huang, J. D. Yao, G. Ning, Q. Xiao and Y. Liu, *Gaodeng Xuexiao Huaxue Xuebao*, 2021, **42**, 2412–2421.

47 F. Gao, F. Liu, X. Bai, X. Xu and M. Li, *Carbon*, 2018, **141**, 331–338.

48 S. Liu, J. Z. Xu and W. G. Zhang, *World J. Microbiol. Biotechnol.*, 2022, **38**, 22.

49 M. Y. Wu, P. Mukherjee, D. N. Lamont and D. H. Waldeck, *J. Phys. Chem. C*, 2010, **114**, 5751–5759.